Optics & Laser Technology 177 (2024) 111069

Contents lists available at ScienceDirect

Optics and Laser Technology

journal homepage: www.elsevier.com/locate/optlastec

Research Note

Controlled photothermal ablative processing of commercial polymers minimizing undesired thermal effects under high frequency femtosecond laser irradiation

A.P. Bernabeu [a], D. Puerto [a,b,*], M.G. Ramirez [a,b], G. Nájar [a], J. Francés [a,b], S. Gallego [a,b], A. Márquez [a,b], I. Pascual [a,c], A. Beléndez [a,b]

[a] I.U. Física Aplicada a las Ciencias y las Tecnologías, Universidad de Alicante, 03690, San Vicente del Raspeig, Spain
[b] Dept. Física, Ingeniería de Sistemas y Teoría de la Señal, Universidad de Alicante, 03690, San Vicente del Raspeig, Spain
[c] Dept. Óptica, Farmacología y Anatomía, Universidad de Alicante, 03690, San Vicente del Raspeig, Spain

A B S T R A C T

The response of three commercial polymers (poly(vinyl chloride) (PVC), poly(ethylene terephthalate) (PET) and polypropylene (PP)) with different thermal properties under high repetition rates (1 kHz-1 MHz) with femtosecond (450 fs) multi-pulse laser irradiation at $\lambda = 515$ nm (1.4 J/cm^2) is reported resulting in a complete study with controlling the ablation depth and minimizing collateral thermal effects. Tunable ablation depth is achieved accurately by varying the repetition rate at a constant fluence. The results are compared to a photothermal model that aims at explaining the heat accumulation effect of successive pulses as a function of the repetition rate and predicts three different heat regimes (non-cumulative, cumulative and saturation). The threshold frequencies for each regime can be estimated from the model, providing control for selecting frequency values and thermal regimes. Thermal analyses are performed to characterize the materials, concluding that thermal parameters are vital for selecting optimal materials and laser processing parameters.

1. Introduction

The importance of polymers has grown enormously over the last decades. Because of their remarkable properties and their low economical cost, these materials have been introduced in a vast number of fields, such as electronics, technological devices, vehicle industry, aeronautics, domestic appliances, medical devices or biomedicine [1–3].

Three of the most commonly used commercial polymers are poly (vinyl chloride) (PVC), poly(ethylene terephthalate) (PET) and polypropylene (PP). PVC is an amorphous polymer whereas PET and PP are semicrystalline polymers. They all can be found in everyday objects and home appliances, such as pipes for potable water (PVC), vehicle components (PP) or as bottles (PET) [4–6]. However, one of the main areas of interest is the use of these materials in the fabrication of flexible electronic and photoelectronic devices [7–10]. In this sense, ultra-short laser sources have been used in order to fabricate optical instruments employing polymers, such as microlenses [11,12], waveguides [13], diffractive gratings [14] or devices like microfluidic channels [15].

The advantages of femtosecond lasers to process materials have attracted much attention over the last decades [16]. Because of their short pulse time, high intensities are produced and non-linear absorption processes are induced. Consequently, absorption is restricted to the focal volume for femtosecond lasers, unlike pico or nanosecond sources [16–19]. Nevertheless, after a succession of ultra-short pulses impinge on the material, the temperature in the absorption zone increases and starts to diffuse, enlarging the damaged area. This effect increases when the time between pulses is small (i.e., due to high repetition rates) and depends on the thermal diffusivity of the processed material [19].

The use of high-frequency lasers (above 1 kHz) allows considerably shorter processing times, which is an advantage for device fabrication [20,21]. However, it has been proved that thermal damage is produced when processing materials at high repetition rate frequencies and powers. [22,23,24]. Therefore, fine control of these parameters is key for the industrial use of ultrashort lasers, as it would allow precise mass production.

To develop reliable devices based on polymers using femtosecond laser techniques, it becomes necessary to know and to control the behavior of these materials at different laser parameters. First studies on laser irradiation on polymers were performed for nanosecond UV sources and low repetition rates [25–28] describing the presence of surface etching and its dependence on laser intensity and number of

* Corresponding author at: I.U. Física Aplicada a las Ciencias y las Tecnologías, Universidad de Alicante, 03690, San Vicente del Raspeig, Spain.
E-mail address: dan.puerto@ua.es (D. Puerto).

https://doi.org/10.1016/j.optlastec.2024.111069
Received 30 October 2023; Received in revised form 7 April 2024; Accepted 22 April 2024

pulses. Later on, the surface morphology and the ablation depth dependence on laser fluence and pulse duration were also studied with ultra-short UV, visible and IR lasers at low repetition rates [29–31]. It was found that the ablation threshold is reduced significantly with ultra-short sources processing.

Recently, polymer thermal effects under high repetition rate irradiation have been investigated [14,32] and applied to produce linear periodic patterns on polymer surfaces. The effect of repetition rate frequency on heat accumulation has also been modelled for dielectrics and polymers [20,33–37]. The latter studies are mainly focused on the changes produced when the number of pulses is increased for different materials. However, they do not provide results across a broad frequency range. Specifically, the frequency ranges considered in these studies are from 100 kHz to 1 MHz for glasses [20], from 1 kHz to 100 kHz for polyimide and polymethylmethacrylate-based polymers [35], or involve single frequency analyses [33,34,36,37]. Thus, there is a notable absence of studies of the behavior of polymers under ultra-short pulse irradiations for repetition rates ranging from kHz to MHz. The correlation between increasing repetition rate and heat accumulation effects should also be examined in relation to the behavior of these materials [38].

A complete study of the response of PVC, PET and PP under femtosecond laser irradiation for $\lambda = 515$ nm is presented here, with particular emphasis on the dependence of the resulting effects on the repetition rate frequency. The repetition rate window explored ranges from 1 kHz until 1 MHz and the resulting modifications are determined experimentally, obtaining controllable ablation depth at the micrometric scale. An analytical photothermal model is implemented and used to relate experimental results to heat accumulation effects. Different thermal regimes are observed experimentally, which are in good agreement with the predictions from the model. Thermal analyses for the three materials are performed in order to understand their behavior under different irradiations.

2. Experimental setup

The laser system consists of an NKT aeroPULSE FS50 fiber laser that delivers 450 fs laser pulses with an average power up to 50 W at the central wavelength of 1030 nm. Through a frequency-doubling unit, 515 nm can also be achieved. Repetition rates can be tuned between 500 Hz and 2 MHz for each wavelength. The working fluence that we apply in the present work is 1.4 J/cm^2. A fluence test was performed in order to determine a suitable value. The chosen fluence value is above the single pulse modification threshold but not too high to produce large extended thermal damage for the three materials (see supplementary material). The system includes a scanner that controls the X-Y position of the laser beam over the processing material surface. The scanner working velocity values can be set between 1 mm/s and 5 m/s. The scanner also contains a F-theta lens (170 mm effective focal length) to focus the beam, leading to a radius of 9 μm at $1/e^2$ for 515 nm. The radius has been obtained from a representation of the square of the diameter of single pulse ablation craters as a function of the natural logarithm of the laser pulse energy, proposed by Liu et al. [39]. A representation of the experimental setup is presented in Fig. 1.

The samples used in this study are thin films (300 μm thick) of PVC, PET and PP. The bandgaps for each polymer are obtained from absorption spectra and are presented in Table 1. Both, modulated differential scanning calorimetry (MDSC) and thermogravimetry (TG) measurements are performed and showed in Fig. 2. From these analyses, the glass transition (T_g), melting (T_m) and decomposition (T_d) temperatures are obtained. In order to correctly identify the T_d values, the derivative thermogravimetric curves (DTG) are determined from TG results and shown also in Fig. 2. Glass transition refers to the glass-rubbery phase change, melting means crystalline-amorphous transition and decomposition refers to the process by which chemical degradation is produced by heating. The crystallization processes are also

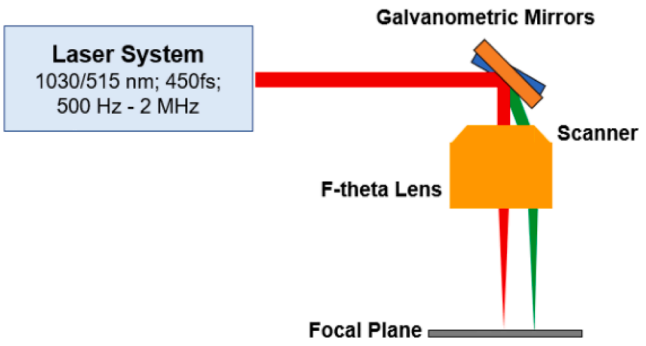

Fig. 1. Sketch of the used experimental setup formed by a femtosecond laser (450 fs, wavelength of 515 nm and 1030 nm), a galvanometric mirrors scanner and an F-theta lens.

Table 1
Bandgaps obtained from absorbance spectra, T_g, T_m, T_d, heat capacity at T_d, thermal conductivities and densities for PVC, PET and PP.

Polymer	Bandgap (eV)	T_g (°C)	T_m (°C)	T_d (°C)	C_p at T_d (J/kgK)	k (W/mK)	ρ (g/cm^3)
PVC	3.95	72.29	–	225	1568	0.137	1.41
PET	3.80	75.55	245.45	349	1979	0.233	1.34
PP	4.00	< 0	157.96	320	2928	0.191	0.95

observed for PET (116 °C) and PP (213 °C). Heat capacity values (C_p) from 25 °C up to the decomposition temperature for each polymer are also obtained from MDSC. Thermal conductivity (k) and material density (ρ) are also measured at 25 °C. All these temperatures, the heat capacities at the decomposition temperature (as an illustrative value), the thermal conductivities and material densities are presented in Table 1. We note that the thermal diffusivity D of these materials, to be introduced in Section 3.2, can be calculated as $D = k/(C_p\,\rho)$.

3. Photothermal hypotheses

Femtosecond laser sources are able to to reach high intensities in the focal volume that may induce non-linear absorption processes. This opens a wide window of processing transparent materials, such as glasses or polymers.

The values of the bandgaps for the three polymers (see Table 1) and our laser wavelength ($\lambda = 515$ nm being equivalent to 2.40 eV) suggest that for these materials, two-photon absorption must be the dominant absorption mechanism.

Under high intensity irradiations, materials are photochemically and photothermally damaged and permanent changes can be induced leading to reflectivity variations associated to phase changes. When the laser intensity is high enough, ablation can be achieved. After these changes are produced in the irradiation area, heat diffusion further expands the damaged area leading to changes outside of the focus position in the material [19]. The impact of this expansion depends on the thermal parameters of each material and the affected area becomes larger as the pulse duration increases.

The repetition rate is an important factor for understanding heat transfer in laser-matter interaction. From a photothermal approach, a high repetition rate might produce an increase of the temperature if the time between pulses is short enough compared to the diffusion time of the material, giving rise to greater changes on the surface of the material [20,21,33]. This is known as the repetition rate effect [40]. The benefits of processing materials with extremely high frequencies, such as reducing processing times, achieving more uniform ablation and decreasing collateral damage from heat accumulation have been reported [22]. A strong advantage of working with polymers that present a

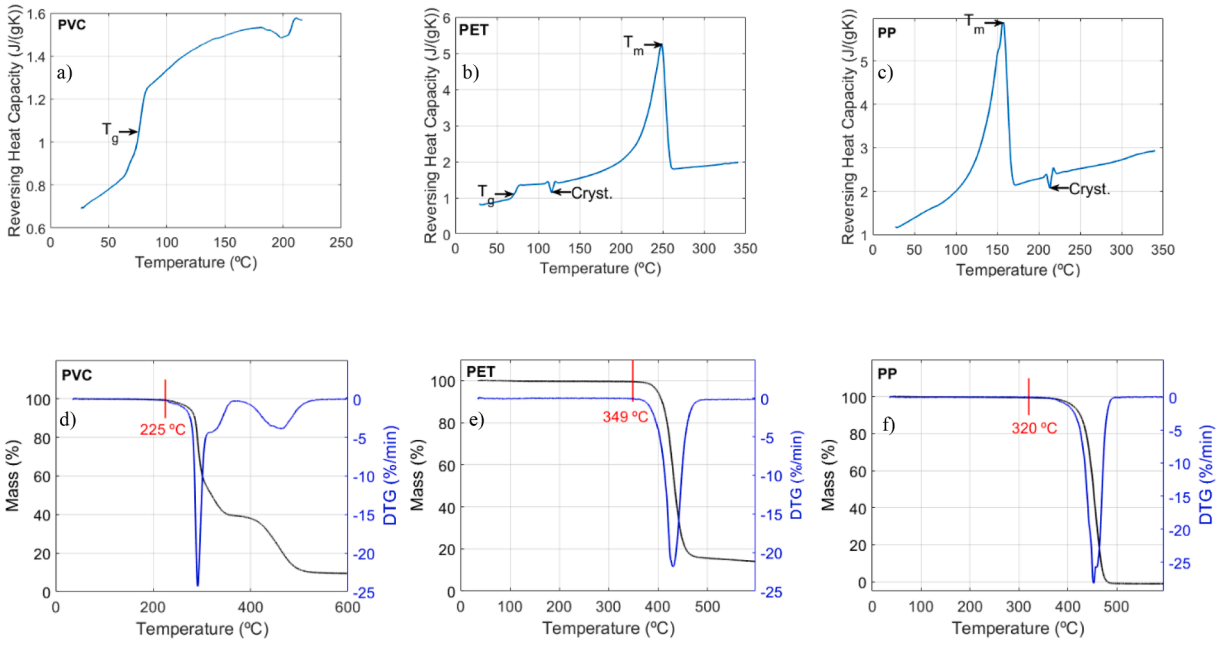

Fig. 2. MDSC curves for PVC (a), PET (b) and PP (c). T_g, T_m and crystallization processes are indicated with arrows. Thermogravimetry (TG, in black), derivative thermogravimetric curves (DTG, in blue) and decomposition temperatures (in red) for PVC (d), PET (e) and PP (f). (For interpretation of the references to colour in this figure legend, the reader is referred to the web version of this article.)

low thermal diffusivity is that these effects related to the laser repetition rate frequency occur at much lower frequency values than for other materials.

Depending on the repetition rate value and the thermal diffusion of the material, two different regimes have been reported [14,19]: For low frequencies, the time between pulses is large enough, so the material is able to diffuse the heat before the next pulse arrives thus reaching the ambient temperature. This is the so-called non-cumulative regime. If the frequency is increased, the time between pulses becomes shorter and diffusion is less efficient. Thus, when the following pulse interacts with the material, the material temperature is above the ambient temperature producing a cumulative heat effect as each pulse arrives. This is known as cumulative regime.

However, for even higher frequencies, we hypothesize a new scenario. If the time between pulses becomes extremely short, the temperature of the material remains essentially constant until the next pulse arrives. Therefore, no matter how much the frequency is increased, heat accumulation will lead to almost the same temperature. This phenomenon gives rise to a thermal saturation, which may manifest as the repetition rate is increased, introducing another thermal regime.

Another hypothesis we propose is that this thermal saturation could be correlated with an ablation saturation effect. Ablation is a very complex phenomenon that depends not only on temperature, but on many different variables. However, in order to get a simple way to predict the dependence of ablation depth on repetition rate, we hypothesize a connection between ablation depth and temperature. This implies that if a temperature saturation is produced at a specific repetition rate, the ablation depth should saturate for a similar range of repetition rates. For this reason, a quantification of the thermal saturation frequency of a given material allows to obtain more control on the efficiency for processing materials. This saturation effect has only been reported for paint [40], but a clear explanation of its appearance is not given.

4. Thermal model

For a better understanding of these thermal processes, we have implemented a simple model based on the solution of the heat diffusion equation reported by the Shimizu et al. [36], detailed in the supplementary material. The most important advantage of this approach is that this model offers a simple analytical solution that – in contrast to a finite difference model – allows a very direct prediction of the frequency for which cumulative and thermal saturation regimes begin.

The heat diffusion equation relates the temporal and spatial evolution of the material temperature:

$$\frac{\partial T(x,t)}{\partial t} = D\frac{\partial^2 T(x,t)}{\partial x^2}, \tag{1}$$

where D is the thermal diffusivity of the material. The resulting temperature increases instantly each time a pulse arrives as $\Delta T_0(x,t) = AE(x,t)/(C_p\rho)$, where A is the estimated energy fraction absorbed by each polymer, $E(x,t)$ is the gaussian laser energy density distribution, ρ is the material density and C_p is the heat capacity of the material. After a pulse absorption, the temperature starts to decrease due to heat diffusion. This mechanism is repeated periodically with the following pulses arrivals.

The proposed solution to equation (1) considering 2D surface heat diffusion is the following [36]:

$$\Delta T(t,r) = \Delta T_0 \frac{(\omega/2)^2}{(\omega/2)^2 + 4Dt}\exp\left[-\frac{r^2}{(\omega/2)^2 + 4Dt}\right], \tag{2}$$

where ω is the laser spot radius at $1/e^2$, t is the diffusion time after a pulse arrives and r is the radial distance to the central point of the spot. To calculate the temperature of the material surface when the next pulse arrives, time must be set to the inverse of the repetition rate frequency ($t = 1/f$).

The results from the thermal analysis between 25 °C and the decomposition temperature for each material (see Fig. 2) are also used to implement the model with heat capacity and thermal diffusion variations. This implies that phase changes that are produced below T_d are considered by the model. Beyond T_d, thermal parameters are implemented as constants and set to their value at T_d. Density, fractions of absorbed energy and thermal conductivity are taken as constants for each material. However, all these thermal and mechanical parameters depend on temperature and might change considerably, especially for

high temperatures. Within this context being aware of all these approximations and that there are more complete approaches [41], the main purpose of this model is to reproduce the dependence of temperature on repetition rate explaining the three thermal regimes, estimating the threshold frequencies for these regimes and building a link between ablation depth and temperature.

5. Results and discussion

5.1. Thermal regimes explanation

As it was mentioned above, three different thermal regimes depending on the repetition rate frequency can be distinguished. The main advantage of the model described in the previous section is that due to its analytical solution to equation (1) an estimation of the threshold frequencies for the cumulative and saturation regimes can be done. For a simpler description of the three regimes, we consider the simpler case of static irradiations (i.e., the laser spot is not moving along the sample).

The repetition rate that indicates the beginning of the accumulation regime and can be estimated setting equation (2) equal to 1 % of the ΔT_0 value. For static irradiations and focusing on the central point ($r = 0$) the cumulative frequency becomes:

$$f_C = \frac{16D}{99\omega^2}, \tag{3}$$

where D is the thermal diffusion of the material and ω is the radius of the laser beam. Thermal diffusivity is obtained experimentally from heat capacity, density and thermal conductivity measures for PVC, PET and PP, as shown in Section 2, and it is temperature dependent. Since at the threshold of the cumulative regime the temperatures reached are not very large, we have taken the value of D at ambient temperature. As a result, the values of f_C obtained for PVC, PET and PP are 281 Hz, 420 Hz and 340 Hz, respectively. It must be noted that the working repetition rates (1 kHz up to 1 MHz) are above f_C, so thermal accumulation effects due to the repetition rate become relevant.

Moreover, it is possible to estimate a thermal saturation frequency (f_{sat}) from the model (Eq. (S5) in supplementary material). This value also depends on the thermal parameters, that vary with temperature and on the number of pulses. In this case, for estimating f_{sat}, thermal parameters values are taken at T_d for each material in order to obtain the saturation frequency from simple analytical equations. The main reason of this assumption is that T_d is exceeded with 30 pulses for all the three materials at high frequencies, so the thermal parameters values are set to their values at T_d.

For static irradiations and considering the value at T_d of the thermal diffusivity and heat capacity for each material, the frequency value that guarantees that the reached temperature at the central point is 90 % of the maximum possible temperature can be defined as the thermal saturation frequency. These frequencies ensure that thermal saturation regime is reached for a given fluence and number of pulses. The so-obtained thermal saturation frequencies for the laser working conditions are 79 kHz, 122 kHz and 98 kHz for PVC, PET and PP, respectively for 30 pulses. For 75 pulses the saturation frequencies are 96 kHz, 141 kHz and 112 kHz for PVC, PET and PP, respectively. The values for 150 pulses are 102 kHz, 148 kHz and 117 kHz for PVC. PET and PP, respectively (see supplementary material).

In addition, the simple model described above is able to estimate the temperature reached as a function of time for a given number of laser pulses irradiated at a given repetition rate. In Fig. 3, the temperature profile simulations are presented for PVC static irradiations at the central point during 30 pulses at 50 Hz, 300 Hz (near above f_C) and 80 kHz (near above f_{sat}). The 50 Hz case shows a non-cumulative regime behavior. Pulses are separated long enough not to produce heat accumulation effects. For 300 Hz thermal accumulation begins to be relevant. These results are compatible with the cumulative frequency calculated above ($f_c = 281$ Hz). In the 80 kHz simulation, time between pulses is so short that diffusion after pulses is not efficient, so temperature remains essentially constant until the next pulse arrives. This can be noted because the temperature profile looks like a Heaviside function, indicating the entrance to the saturation regime at the estimated saturation frequency ($f_{sat} = 79$ kHz). Therefore, using this model, a clear explanation of the three different regimes appears naturally. Similar results are obtained for PET and PP, presenting heat accumulation and

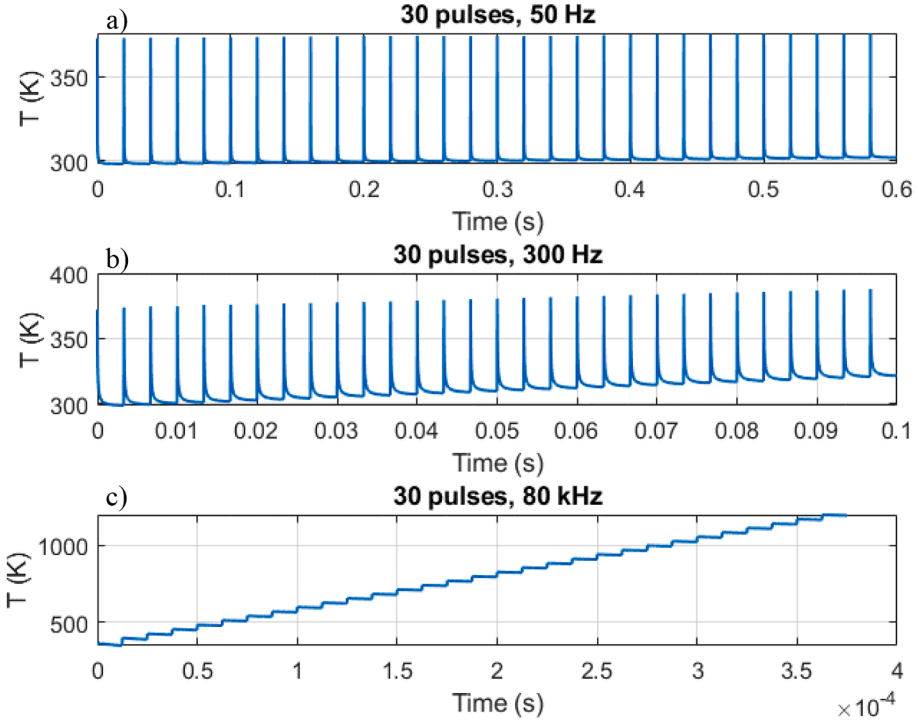

Fig. 3. Simulations of PVC temperature profile for 10 pulses and 50 Hz (a), 300 Hz (b) and 80 kHz (c) for static irradiations.

thermal saturation at the frequencies computed previously.

5.2. Thermal and ablation regimes comparison

Different series of irradiated lines for different number of (partially overlapping) pulses per spot area (30, 75 and 150) for PVC, PET and PP have been performed. For each series of lines with a constant number of pulses per spot area, each line is made with a different repetition rate ranging from 1 kHz to 1 MHz, making the total number of pulses per spot area constant by changing the scanning speed.

Ablation is the main consequence for all the different conditions, as it can be seen in Figs. 4, 5 and 6 (a) for irradiations in the three materials at 1.4 J/cm^2 and N = 150 pulses per spot area. In these images, two facts can be noted: On the one hand, the modified area increases with the frequency for the three materials. It is also evident that the differences between the modified widths of consecutive lines decrease with increasing repetition rate. For instance, the variation in the modification widths between the first and second lines is considerably larger than between the second and third lines. These variations between adjacent lines are greater for PVC and PET than for PP because of their different thermal properties, as explained further down. Indeed, important differences can be observed with lines processed at high frequencies (Fig. 4 (b), 5 (b) and 6 (b)) and with the ones irradiated at low frequencies (Fig. 4 (c), 5 (c) and 6 (c)) at 150 pulses/spot area. For the three materials, the 1 MHz lines present more homogeneity and less debris than the 15 kHz lines. The reduction of the presence of debris at high frequencies has also been reported on steel [42]. The PP case must be emphasized, for which the 1 MHz line (Fig. 6 (b)) presents a notable uniformity and an absence of debris leading to a controllable processing width. These facts expose the benefits of processing materials at high frequencies [22]. On the other hand, there are remarkable differences between the shape of the lines for the three materials. The damaged surface width is bigger for PVC and PET than for PP. In addition, in the surroundings of the ablated region, greater changes in the reflectivity appear for PVC and PET, especially for the latter. PP does not present these reflectivity changes; thus, the ablated line is precisely confined within the designed laser trajectory.

There are two possible explanations for the width and reflectivity differences between the materials. The first one is related to the thermal and optical parameters of the materials. As it is presented in Table 1, the heat capacity at.

T_d is much larger for PP than for PVC and PET. This means that PP needs more energy to increase its temperature and this might lead to a lower ablation rate. Furthermore, according to Fig. 2 (c) the heat capacity for PP has an increasing tendency for higher temperatures, so this effect might be magnified for temperatures beyond T_d. This could lead to a lower heat transfer efficiency for PP that results in a smaller modified width. This effect may be amplified by the greater bandgap presented by PP, that is associated to a lower energy absorption.

The second explanation is based on the phase transitions experienced by each material. In Fig. 2 and Table 1, the corresponding phase transition temperatures for the three materials are shown. PVC and PET present a glass transition temperature about 70 °C, so this phase change can be produced when these materials are processed. However, the glass transition temperature for PP is below 0 °C. Therefore, this transition will not take place for PP. Thus, these extended reflectivity changes might be attributed to the glass transitions that become relevant for points outside the focal volume, where the reached temperatures are below the decomposition temperatures, but might be high enough to produce the phase transition. This phase change increases the volume of the material extending these thermal effects. After heat diffusion, the new state resolidifies and causes a change in the refractive index [14,19,20,30,31]. This explains why reflectivity changes appear only for PVC and PET and increases the damaged area for these two materials. In addition, MDSC results (see Fig. 2 (b)) show that PET presents a crystallization process at 116 °C that might increase the presence of

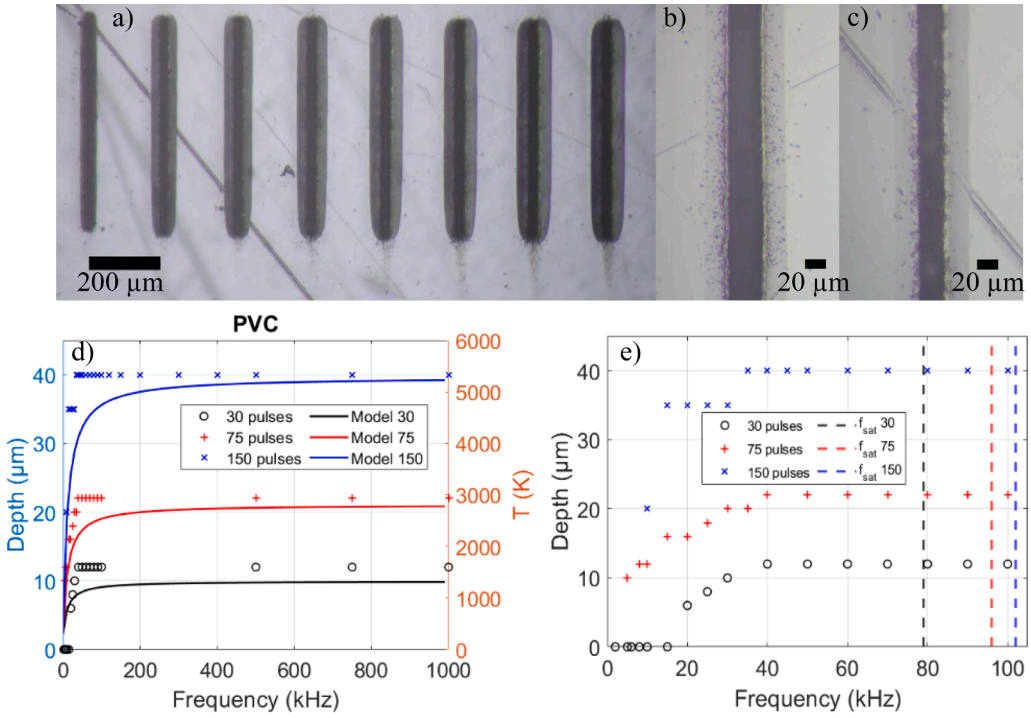

Fig. 4. (a) PVC irradiations at 515 nm with N = 150 pulses and f = 10–45 kHz increasing from left to right. Enlarged images of an irradiated line of 150 pulses/spot area at 1 MHz (b) and 15 kHz (c) for PVC. (d) Measured irradiated lines depth (markers, left axis) and temperature simulations at the center of the spot for static irradiations solid lines, right axis) for 30 pulses (black), 75 pulses (red) and 150 pulses (blue)/spot area as a function of repetition rate for PVC. (e) Measured irradiated lines depth (markers) and estimated saturation frequencies (dashed lines) for 30 pulses (black), 75 pulses (red) and 150 pulses (blue)/spot area as a function of repetition rate for PVC.

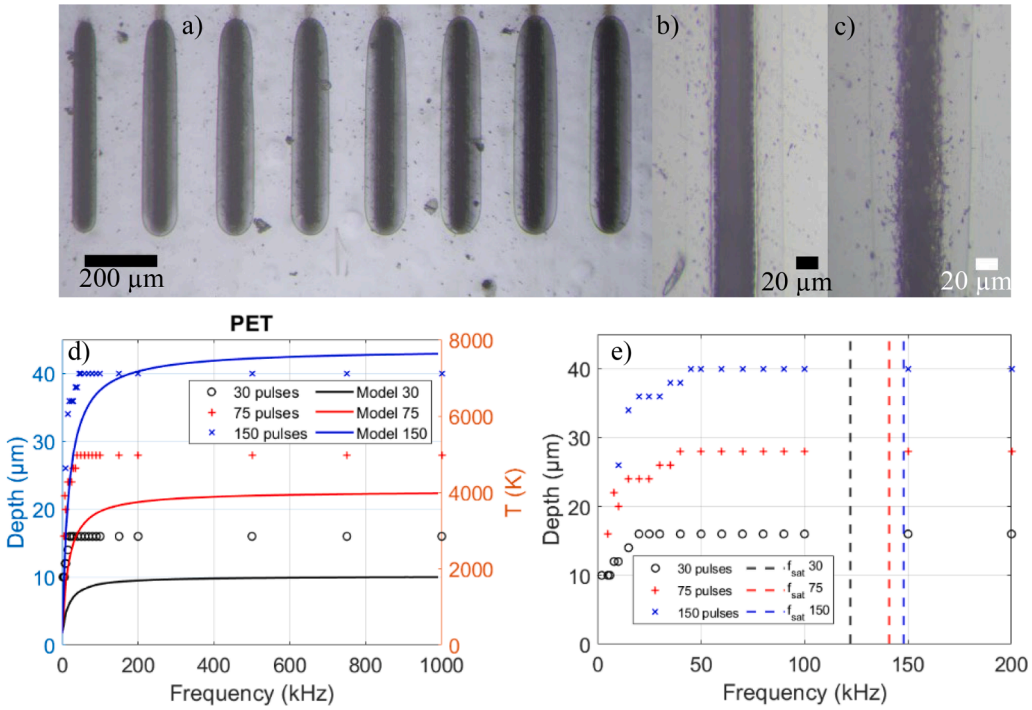

Fig. 5. (a) PET irradiations at 515 nm with N = 150 pulses and f = 10–45 kHz increasing from left to right. Enlarged images of an irradiated line of 150 pulses/spot area at 1 MHz (b) and 15 kHz (c) for PET. (d) Measured irradiated lines depth (markers, left axis) and temperature simulations at the center of the spot for static irradiations (solid lines, right axis) for 30 pulses (black), 75 pulses (red) and 150 pulses (blue)/spot area as a function of repetition rate for PET. (e) Measured irradiated lines depth (markers) and estimated saturation frequencies (dashed lines) for 30 pulses (black), 75 pulses (red) and 150 pulses (blue)/spot area as a function of repetition rate for PET.

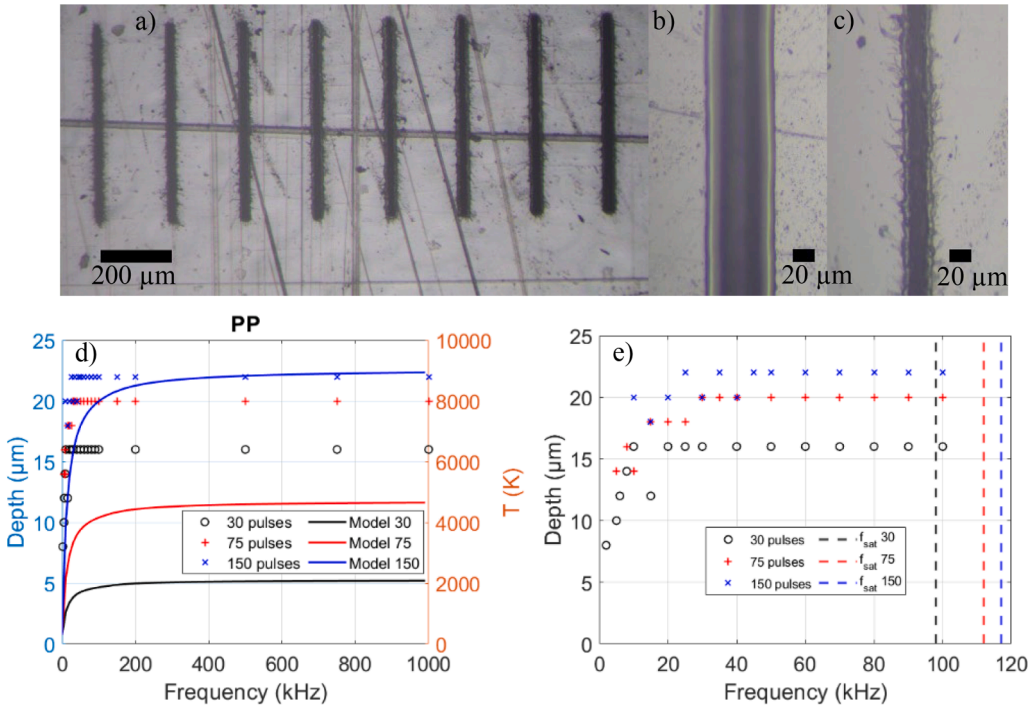

Fig. 6. (a) PP irradiations at 515 nm with N = 150 pulses and f = 10–45 kHz increasing from left to right. Enlarged images of an irradiated line of 150 pulses/spot area at 1 MHz (b) and 15 kHz (c) for PP. (d) Measured irradiated lines depth (markers, left axis) and temperature simulations at the center of the spot for static irradiations (solid lines, right axis) for 30 pulses (black), 75 pulses (red) and 150 pulses (blue)/spot area as a function of repetition rate for PP. (e) Measured irradiated lines depth (markers) and estimated saturation frequencies (dashed lines) for 30 pulses (black), 75 pulses (red) and 150 pulses (blue)/spot area as a function of repetition rate for PP.

surrounding thermal effects and their area, compared to PVC. Melting transitions appear to play a minimal role in enlarging the modified widths as no reflectivity changes are observed in the surroundings of the ablated area for PP.

As mentioned above, the main consequence of processing these materials is ablation. The depth of the produced trenches was measured and the obtained temperature in the center of the spot for each case was calculated through the model that fulfills equations (1) and (2). Results as a function of the repetition rate for the three materials are presented in Fig. 4 (d), 5 (d) and 6 (d) up to 1 MHz. In Fig. 4 (e), 5 (e) and 6 (e), the experimental ablation depths and the simulated thermal saturation frequencies described in Section 4.1 are represented as a function of frequency within a range up to 100–200 kHz. The results indicate that there is an increase in ablation depth with the repetition rate when this parameter is below 50 kHz, approximately. This trend occurs across all the tested number of pulses and materials. For higher frequencies, a saturation is produced, and depth values stay constant. These effects are observed for all the three materials. This result shows that it is possible to obtain a tunable depth at the micron level by changing the repetition frequency at constant fluence.

PET exhibits a slightly greater ablation depth for 30 pulses (16 μm at 1 MHz) and 75 pulses (28 μm at 1 MHz) than PVC, with values of 12 μm for 30 pulses and 22 μm for 75 pulses at 1 MHz. For the PP case, the same ablation depth as with PET is produced for 30 pulses (16 μm at 1 MHz) and a lower ablation depth is presented for 75 pulses (20 μm at 1 MHz) than for PET. This might be related to the PET lower bandgap (see Table 1) that implies a smaller modification threshold (see supplementary material). For 150 pulses, PVC and PET present higher ablation depths than PP. As in the case of the modified width, the higher values of heat capacity and bandgap for PP could lead to a smaller ablation efficiency. In the same way, glass transition suffered by PVC and PET changes the density of the material and could increase the modification and ablation volumes.

The calculated temperatures (solid lines) in Fig. 4 (d), 5 (d) and 6 (d) also describe the temperature increase (until 5226 K for PVC, 7628 K for PET and 8937 K for PP at 150 pulses and 1 MHz) and a thermal saturation effect for the same range of repetition rates as presented by the experimental ablation depth curves. Therefore, simulated temperatures and ablated depths show a similar behavior. This allows to establish a connection between temperature and ablation depth, according to the hypothesis explained above.

In Fig. 4 (e), 5 (e) and 6 (e) the differences between thermal and ablation saturation can be observed. It must be noted that thermal saturation frequencies were defined as the frequencies for which the 90 % of the maximum temperature was reached considering thermal values at T_d. In this way, thermal saturation frequencies ensure that the thermal saturation regime is achieved. However, the ablation saturation occurs at lower frequencies (around 20–50 kHz below) compared to the estimated thermal saturation frequencies. This indicates that ablation saturation is produced for a smaller percentage than the 90 % of the maximum temperature. Nevertheless, the estimated thermal saturation frequencies provide a suitable approximation for the frequency ranges for which the ablation saturation is produced. Indeed, considering the simplicity of the model and the geometrical differences (the model considers static irradiations while the real material processing adopts straight-line geometry), it is important to estimate a frequency that guarantees the occurrence of saturation effects. Adjusting the frequency to the estimated saturation frequency offers advantages in efficiency, particularly when aiming to achieve maximum depths under specified conditions of fluence and number of pulses.

Furthermore, in addition to saturation occurring within the correct temperature range for the three materials, the relationship between temperature and ablation depth appears to follow a very similar pattern for PVC and PET. The experimental data points and simulated temperature lines align reasonably well for both materials, indicating a direct correlation between temperature increase and ablation depth for these materials. However, for PP, the simulated temperature lines and ablation depths do not align. Additionally, it is evident that the depths obtained for 30, 75, and 150 pulses are more similar for PP compared to PVC and PET. This suggests that PP exhibits greater resistance to temperature increases, resulting in lower ablation efficiency, as discussed above.

6. Conclusions

The behavior of three commercial polymers has been studied under $\lambda = 515$ nm femtosecond laser irradiation for different repetition rates and different number of pulses per spot area. Ablation is the main type of modification observed in the three materials. The ablation depth increases as repetition rate increases up to a saturation value, enabling a tunability of the micrometric depth value by changing repetition rate at constant fluence. The benefits provided by high frequency processing are enhanced uniformity and small amount of debris. The effect of cumulative pulses is analyzed by measuring the irradiation depths, which are compared with the results of a photothermal model. This offers a simple analytical equation for describing heat diffusion. Repetition rate effects and the three thermal regimes are explained by the model, thus allowing the estimation of the threshold frequencies for cumulative and saturation regimes. The ablation saturation can be determined from an estimation of the thermal saturation frequency, enabling the control of the ablation efficiency. The thermal characterization of polymers is performed by applying MDSC and TG analyses, and thermal conductivity measurements, which are included in the model.

From these results, it becomes clear how important the knowledge of the materials thermal characteristics for predicting is and how important the understanding their behavior under femtosecond laser irradiation is. In this frame, materials with low values of phase transition temperatures could be less suitable for laser processing compared to materials with inexistent, negative or high values for these temperatures. In this case, because of the lack of extended thermal effects that results into ablation lines with high uniformity and a low amount of debris at high frequencies, PP exhibits better qualities for ultrashort laser subtracting manufacturing than PVC and PET for our experimental conditions.

CRediT authorship contribution statement

A.P. Bernabeu: Writing – review & editing, Writing – original draft, Investigation, Data curation. **D. Puerto:** Writing – review & editing, Writing – original draft, Supervision, Investigation, Data curation, Conceptualization. **M.G. Ramirez:** Methodology, Investigation, Conceptualization. **G. Nájar:** Investigation. **J. Francés:** Software, Data curation, Conceptualization. **S. Gallego:** Writing – review & editing, Writing – original draft, Resources, Conceptualization. **A. Márquez:** Writing – original draft, Investigation, Conceptualization. **I. Pascual:** Writing – original draft, Funding acquisition, Conceptualization. **A. Beléndez:** Writing – original draft, Funding acquisition, Conceptualization.

Declaration of competing interest

The authors declare that they have no known competing financial interests or personal relationships that could have appeared to influence the work reported in this paper.

Data availability

No data was used for the research described in the article.

Acknowledgements

The work was supported by the “Generalitat Valenciana”

(IDIFEDER/2021/014 cofunded by FEDER EU program, project PROMETEO/2021/006, and INVESTIGO program (INVEST/2022/419) financed by Next Generation EU), "Ministerio de Ciencia e Innovación" of Spain (projects PID2021-123124OB-I00; PID2019-106601RB-I00), by "Universidad de Alicante'' (UATALENTO18-10). The authors acknowledge helpful discussions with J. Siegel from the Laser Processing Group at IO-CSIC in Madrid.

Appendix A. Supplementary data

Supplementary data to this article can be found online at https://doi.org/10.1016/j.optlastec.2024.111069.

References

[1] K. Modjarrad, S. Ebnesajjad, Handbook of polymer applications in medicine and medical decives, 1st ed., Elsevier, San Diego, CA, USA, 2014.
[2] S. Ramakrishna, J. Mayer, E. Wintermantel, K.W. Leong, Biomedical applications of polymer-composite materials: a review, Compos. Sci. Technol. 61 (9) (2001) 1189–1224, https://doi.org/10.1016/S0266-3538(00)00241-4.
[3] C. Scholz, Polymers for Biomedicine: Synthesis, Characterization, and Applications, 1st ed, John Wiley & Sons, Hoboken, NJ, USA, 2017.
[4] J. Leadbitter, J.A. Day, J.L. Ryan, PVC: Compounds, Processing and Applicattions, Rapra Technology LTd, Shawbury, UK, 1997.
[5] H.A. Maddah, Polypropylene as a promising plastic: A review, Am. J. Polym. Sci. 6 (1) (2016) 1–11, https://doi.org/10.5923/j.ajps.20160601.01.
[6] C.M. Carr, D.J. Clarke, A.D.W. Dobson, Microbial Polyethilene Terephthalate hydrolases: current and future perspectives, Front. in Microbiol. 11 (2020) 1–23, https://doi.org/10.3389/fmicb.2020.571265.
[7] F. Zacharatos, M. Makrygianni, R. Geremina, E. Biver, D. Karnakis, S. Leyder, D. Puerto, P. Delaporte, I. Zergioti, Laser Direct Write micro-fabrication of large area electronics on flexible substrates, Appl. Surf. Sci. 374 (2016) 117–123, https://doi.org/10.1016/j.apsusc.2015.10.066.
[8] D. Puerto, E. Biver, A.-P. Alloncle, P. Delaporte, Single step high-speed printing of continuous silver lines by laser-induced forward transfer, Appl. Surf. Sci. 374 (2016) 183–189, https://doi.org/10.1016/j.apsusc.2015.11.017.
[9] Y. Sun, J.A. Rogers, Inorganic semiconductors for flexible electronics, Adv. Mater. 19 (15) (2007) 1897–1916, https://doi.org/10.1002/chin.200739224.
[10] I. Kang, M.J. Schulz, J.H. Kim, V. Shanov, D. Shi, A carbon nanotube strain sensor for structural health monitoring, Smart Mater. Struct. 15 (3) (2006) 737, https://doi.org/10.1088/0964-1726/15/3/009.
[11] M. Xu, Y. Xue, J. Li, L. Zhang, H. Lu, Z. Wang, Large-Area and Rapid Fabrication of a Microlens Array on Flexible Substrate for an Integral Imaging 3D Display, ACS Appl. Mater. Interfaces 15 (2023) 10219–10227, https://doi.org/10.1021/acsami.2c20519.
[12] C. Zheng, A. Hu, K.D. Kihm, Q. Ma, R. Li, T. Chen, W.W. Duley, Femtosecond laser fabrication ofcavity microball lens (CMBL) inside a PMMA substrate for super-wide angle imaging, Small 11 (25) (2015) 3007–3016, https://doi.org/10.1002/smll.201403419.
[13] P. Bollgruen, T. Wolfer, U. Gleissner, D. Mager, C. Megnin, L. Overmeyer, T. Hanemann, J.G. Korvink, Ink-jet printed optical waveguides, Flex. Print. Electron. 2 (4) (2017) 045003, https://doi.org/10.1088/2058-8585/aa8ed6.
[14] D. Sola, J.R. Vázquez de Aldana, P. Artal, The role of thermal accumulation on the fabrication of diffraction gratings in ophthalmic PHEMA by ultrashort laser direct writing, Polym. 12 (12) (2020) 2965, https://doi.org/10.3390/polym12122965.
[15] R. Suriano, A. Kuznetsov, S.M. Eaton, R. Kiyan, G. Cerullo, R. Osellame, B. N. Chichkov, M. Levi, S. Turri, Femtosecond laser ablation of polymeric substrates for the fabrication of microfluidic channels, Appl. Surf. Sci. 257 (14) (2011) 6243–6250, https://doi.org/10.1016/j.apsusc.2011.02.053.
[16] M. Lenzner, Femtosecond laser-induced damage of dielectrics, Int. J. Mod. Phys. B 13 (13) (1999) 1559–1578, https://doi.org/10.1142/s0217979299001570.
[17] B.C. Stuart, M.D. Feit, A.M. Rubenchik, B.W. Shore, M.D. Perry, Laser-induced damage in dielectrics with nanosecond to subpicosecond pulses, Phys. Rev. Lett. 74 (12) (1995) 2248, https://doi.org/10.1103/physrevlett.74.2248.
[18] A.-C. Tien, S. Backus, H. Kapteyn, M. Murnane, G. Mourou, Short-pulse laser damage in transparent materials as a function of pulse duration, Phys. Rev. Lett. 82 (19) (1999) 3883, https://doi.org/10.1103/physrevlett.82.3883.
[19] H. Misawa, S. Juodkazis, 3D Laser Microfabrication, Wiley-VCH Verlag, Weinheim, Germany, 2006.
[20] S.M. Eaton, H. Zhang, P.R. Herman, F. Yoshino, L. Shah, J. Bovatsek, A.Y. Arai, Heat accumulation effects in femtosecond laser-written waveguides with variable repetition rate, Opt. Exp. 13 (12) (2005) 4708–4716, https://doi.org/10.1364/opex.13.004708.
[21] S.M. Eaton, H. Zhang, M. Ling, J. Li, W.-J. Chen, S. Ho, P.R. Herman, Transition from thermal diffusion to heat accumulation in high repetition rate femtosecond laser writing of buried optical waveguides, Opt. Exp. 16 (13) (2008) 9443–9458, https://doi.org/10.1364/oe.16.009443.
[22] C. Kerse, H. Kalaycıoğlu, P. Elahi, B. Çetin, D.K. Kesim, Ö. Akçaalan, S. Yavaş, M. D. Aşık, B. Öktem, H. Hoogland, R. Holzwarth, F.Ö. Ilday, Ablation-cooled material removal. with ultrafast bursts of pulses, Nat. 537 (7618) (2016) 84–88, https://doi.org/10.1038/nature18619.
[23] S.H. Chung, E. Mazur, Surgical applications of femtosecond lasers, J. Biophotonics 2 (10) (2009) 557–572, https://doi.org/10.1002/jbio.200910053.
[24] F. Bauer, A. Michalowski, T. Kiedrowski, S. Nolte, Heat accumulation in ultra-short pulsed scanning laser ablation of metals, Opt. Exp. 23 (2) (2015) 1035–1043, https://doi.org/10.1364/OE.23.001035.
[25] R. Srinivasan, V. Mayne-Banton, Self-developing photoetching of poly (ethylene terephthalate) films by far-ultraviolet excimer laser, Appl. Phys. Lett. 41 (6) (1982) 576–578, https://doi.org/10.1063/1.93601.
[26] Y. Kawamura, K. Toyoda, S. Namba, Effective deep ultraviolet photoetching of polymethyl methacrylate by an excimer laser, Appl. Phys. Lett. 40 (5) (1982) 374–375, https://doi.org/10.1063/1.93108.
[27] S. Lazare, R. Srinivasan, Surface properties of poly (ethylene terephthalate) films modified by far-ultraviolet radiation at 193 nm (laser) and 185 nm (low intensity), J. Phys. Chem. 90 (10) (1986) 2124–2131, https://doi.org/10.1021/j100401a028.
[28] H. Watanabe, M. Yamamoto, Laser ablation of poly (ethylene terephthalate), J. Appl. Polym. Sci. 64 (6) (1997) 1203–1209, https://doi.org/10.1002/(sici)1097-4628(19970509)64:6<1203::aid-app21>3.0.co;2-v.
[29] A.A. Serafetinides, M.I. Makropoulou, C.D. Skordoulis, A.K. Kar, Ultra-short pulsed laser ablation of polymers, Appl. Surf. Sci. 180 (1–2) (2001) 42–56, https://doi.org/10.1016/s0169-4332(01)00324-5.
[30] A.A. Serafetinides, C.D. Skordoulis, M.I. Makropoulou, A.K. Kar, Picosecond ans subpicosecond visible laser ablation of optically transparent polymers, Appl. Surf. Sci. 13 (1–4) (1998) 276–284, https://doi.org/10.1016/s0169-4332(98)00276-1.
[31] X. Liu, D. Du, G. Mourou, Laser ablation and micromaching with ultrashort laser pulses, IEEE J. of Quant. Electron. 33 (10) (1997) 1706–1716, https://doi.org/10.1109/3.631270.
[32] D. Sola, R. Cases, High-repetition-rate femtosecond laser processing of acrylic intra-ocular lenses, Polym. 12 (1) (2020) 242, https://doi.org/10.3390/polym12010242.
[33] C.B. Schaffer, J.F. García, E. Mazur, Bulk heating of transparent materials using a high-repetition-rate femtosecond laser, Appl. Phys. A 76 (2003) 351–354, https://doi.org/10.1007/s00339-002-1819-4.
[34] C.B. Schaffer, A. Brodeur, J.F. García, E. Mazur, Micromachining bulk glass by use of femtosecond laser pulses with nanojoule energy, Opt. Lett. 26 (2) (2001) 93–95, https://doi.org/10.1364/ol.26.000093.
[35] F.C. Burns, S.R. Cain, The effect of pulse repetition rate on laser ablation of polyimide and polymethylmethacrylate-based polymers, J. Appl. Phys. D 29 (5) (1996) 1349, https://doi.org/10.1088/0022-3727/29/5/034.
[36] M. Shimizu, M. Sakakura, M. Ohnishi, Y. Shimotsuma, T. Nakaya, K. Miura, K. Hirao, Mechanism of heat-modification inside a glass after irradiation with high-repetition rate femtosecond laser pulses, J. Appl. Phys. 108 (7) (2010) 073533, https://doi.org/10.1063/1.3483238.
[37] E.G. Gamaly, A.V. Rode, B. Luther-Davies, Ultrafast ablation with high-pulse-rate lasers. Part I: Theoretical considerations, J. Appl. Phys. 85 (8) (1999) 4213–4221, https://doi.org/10.1063/1.370333.
[38] S. Ravi-Kumar, B. Lies, X. Zhang, H. Lyu, H. Qin, Laser ablation of polymers: A review, Polym. Int. 68 (8) (2019) 1391–1401, https://doi.org/10.1002/pi.5834.
[39] J.M. Liu, Simple technique for measurements of pulsed Gaussian-beam spot sizes, Opt. Lett. 7 (5) (1982) 196–198, https://doi.org/10.1364/ol.7.000196.
[40] F. Brygo, C. Dutouquet, F. Le Guern, R. Oltra, A. Semerok, J.M. Weulersse, Laser fluence, repetition rate and pulse duration effects on paint ablation, Appl. Surf. Sci. 252 (6) (2006) 2131–2138, https://doi.org/10.1016/j.apsusc.2005.02.143.
[41] L.L. Taylor, J. Qiao, J. Qiao, Optimization of femtosecond laser processing of silicon via numerical modeling, Opt. Mat. Exp. 6 (19) (2016) 2745–2758, https://doi.org/10.1364/OME.6.002745.
[42] C. Florian, Y. Fuentes-Edfuf, E. Skoulas, E. Stratakis, S. Sanchez-Cortes, J. Solis, J. Siegel, Influence of Heat Accumulation on Morphology Debris Deposition and Wetting of LIPSS on Steel upon High Repetition Rate Femtosecond Pulses Irradiation, Mat. 15 (2022) 17468, https://doi.org/10.3390/ma15217468.